International Journal of Microwave and Wireless Technologies

cambridge.org/mrf

Ultracompact isolated multilayer broadside-coupled balun with arbitrary isolation bandwidth

Masoud Farhadinia, Shokrollah Karimian and Esfandiar Mehrshahi

School of Electrical Engineering, Shahid Beheshti University

Research Paper

Cite this article: Farhadinia M, Karimian S, Mehrshahi E (2024) Ultracompact isolated multilayer broadside-coupled balun with arbitrary isolation bandwidth. *International Journal of Microwave and Wireless Technologies*, 1–9. https://doi.org/10.1017/S1759078724000709

Received: 17 February 2024
Revised: 22 May 2024
Accepted: 27 May 2024

Keywords:
impedance transformation; multilayer broadside-coupled balun; power combiners/dividers; push-pull amplifiers; wideband isolation circuit

Corresponding author: S. Karimian; Email: s_karimian@sbu.ac.ir

Abstract

An isolated low-profile multilayer all-ports-matched broadside-coupled balun (BCB) with arbitrary isolation bandwidth is presented. Analytical relations are derived and provided for the isolation circuit (IC) design in terms of electrical and physical parameters. Accordingly, instructions are given on obtaining optimum bandwidth and isolation responses for the IC. Design procedure for the BCB is presented together with a case study for power amplifier application. The BCB is validated theoretically, analytically, and experimentally, and results are in good agreement. The fabricated balun has insertion loss of 0.27 dB, input and output return losses of 19 dB, isolation of 20 dB at f_c, and phase and magnitude imbalance better than 2° and 0.2 dB across the Bandwidth (BW), respectively. The realized isolated balun has dimensions of $0.06\lambda_g \times 0.03\lambda_g$.

Introduction

Baluns are used to divide an unbalanced signal into a pair of out-of-phase (balanced) signals and transform impedance; and thus, they find application in diverse microwave circuits, such as power amplifiers (PAs) [1–5], balanced mixers [6], frequency multipliers, and antenna feeding networks [7]. Microwave baluns have been realized using coaxial cables [8], multilayer coupled structures [9], and spiral coils [10].

Planar Marchand balun (MB) seems to be the most popular balun due to its simplicity, wideband performance and manufacturing benefits. However, MB structure occupies large circuit area [11, 12]. Unlike MB, the broadside-coupled balun (BCB), which relies on inductive coupling, reduces balun size considerably [9]. The low-profile and step-down impedance transformation of the latter makes it extremely suitable for power division/combining, particularly in push-pull PAs. However, for PAs, isolation and output matching are very crucial to improve reliability. In fact, without isolation circuit (IC), the reflected power at output ports of transistors would damage the transistor as a result of amplitude imbalance at output ports. Regardless of the type of balun, research on microwave baluns has mainly focused on techniques to reduce size [13, 14], broaden bandwidth [15], and lower insertion loss [16], but little has been written on isolation of baluns.

The isolation of a MB was first addressed in paper [12], where the IC included a $\lambda/2$ transmission line (TL), making it both narrowband and lengthy. Later, wideband and compact ICs were proposed [11, 17]. Nevertheless, to the best of authors' knowledge, isolation in BCBs is not well-explored.

In this paper, a multilayer highly isolated BCB is designed that benefits from new embedded compact wideband IC. The novelty and contribution of this work includes: (a) offering new simple compact IC with arbitrary isolation bandwidth, (b) providing analytical relations for synthesis of the IC as well as systematic approach for designing the balun itself, (c) offering analytical relations and instructions on obtaining optimum bandwidth and isolation responses for the IC, and validating it numerically, through full-wave simulation, and experimentally via fabrication, and (d) presenting a worked example through a case study for PA application. In doing so, "Analysis of the isolated BCB" presents the analysis of isolated BCB and the IC."Design of the isolated BCB" offers design procedure and synthesis through a case study. Closed-form formula and considerations for design of the isolated BCB are also presented. This section also evaluates balun power handing capability (PHC) constrains and tunability in design of such balun. Simulation and measurement results are given in "Simulation and measurement" and conclusions are drawn in "Conclusion".

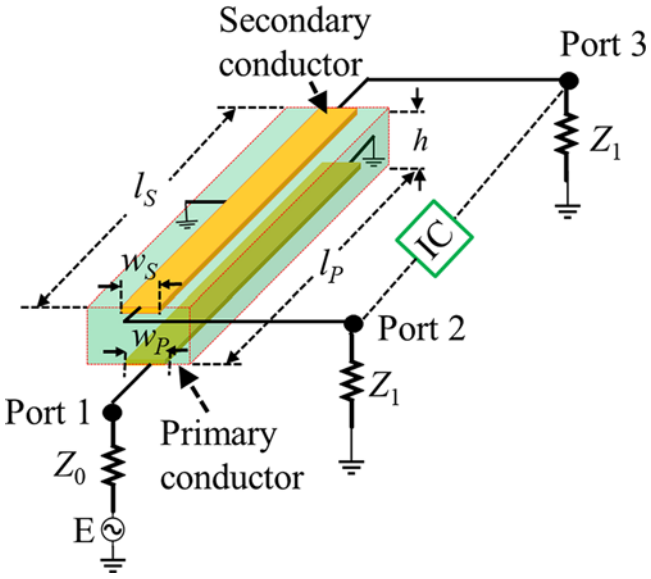

Figure 1. Broadside-coupled balun with isolation circuit.

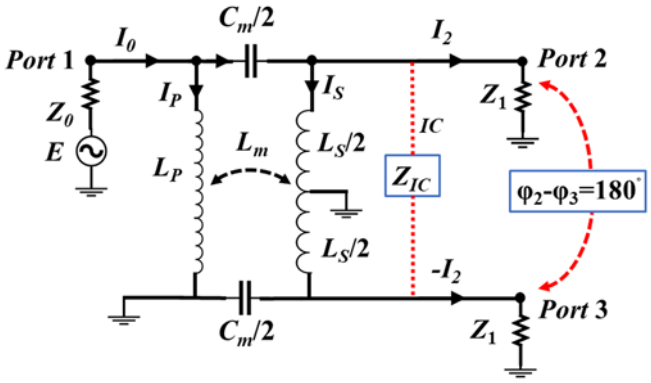

Figure 2. Equivalent circuit model of balun of Figure 1.

Analysis of isolated BCB

Theory of operation

As seen in Fig. 1, a BCB is formed of two conductors sandwiched by a substrate, with l_P, l_S, w_P, and w_s as lengths and widths of primary (bottom) and secondary (top) conductors, respectively. In addition, h is the substrate thickness. When port 1 is excited, power is transferred from the bottom conductor to the top conductor into ports 2 and 3 [18]. BCB, however, suffers from poor isolation between output ports [19]. Therefore, an IC is placed between ports 2 and 3 to achieve good isolation response.

Figure 2 represents the equivalent circuit model of the BCB of Fig. 1 [20]. The BCB can be modelled by a transformer comprised of primary inductor, L_P, secondary inductor, L_s, and mutual inductance and capacitance denoted by L_m, and C_m, respectively. In addition, Z_0: port 1 impedance, Z_1: ports 2 and 3 impedances, I_P: current of primary inductor, I_S: current of secondary inductor, and I_0: current at input port. Ohmic and dielectric losses are neglected for simplicity.

Mutual inductance, L_m, can be determined as a function of self-inductances, L_P and L_S, such that $L_m = K_m\sqrt{L_P L_s}$, where K_m is the magnetic coupling coefficient. Equation (1) expresses impedance transformation ratio ($2Z_1/Z_0$) in terms of primary and secondary inductors.

$$\frac{2Z_1}{Z_0} = K_m{}^2\frac{L_s}{L_p} = \frac{1}{n^2} \cong \left(\frac{N_s}{N_p}\right)^2 \tag{1}$$

where N_P and N_s are number of turns for primary and secondary windings, respectively. Also, n is the ratio of primary to secondary turns [21].

Extracting the S-matrix of isolated balun

Under the lossless condition and neglecting magnetic flux leakage, the S-matrix of the balun of Fig. 1, without the IC, can be given by [19]:

$$[S] = \begin{bmatrix} 0 & j/\sqrt{2} & -j/\sqrt{2} \\ j/\sqrt{2} & 1/2 & 1/2 \\ -j/\sqrt{2} & 1/2 & 1/2 \end{bmatrix} \tag{2}$$

As equation (2) implies, while the input port is matched, the output ports are not matched without the IC. Return losses of output ports (S_{22}, S_{33}) and isolation between them (S_{32}) are 6 dB; emphasizing the need for an IC. The S-matrix of the balun with IC can be obtained if admittance matrix (Y-matrix) of the balun without IC is calculated based on port designations in Fig. 1, as:

$$[\mathrm{Y}]_{\text{without IC}} = \left(y^* - \mathrm{y}\mathrm{k}^{-1}\mathrm{S}k^*\right)\left(\mathrm{k}^{-1}\mathrm{S}k^* + \mathrm{U_n}\right)^{-1} = \begin{bmatrix} 0 & \frac{-\mathrm{j}}{\sqrt{2Z_0Z_1}} & \frac{\mathrm{j}}{\sqrt{2Z_0Z_1}} \\ \frac{-\mathrm{j}}{\sqrt{2Z_0Z_1}} & 0 & 0 \\ \frac{\mathrm{j}}{\sqrt{2Z_0Z_1}} & 0 & 0 \end{bmatrix} \tag{3}$$

https://doi.org/10.1017/S1759078724000709 Published online by Cambridge University Press

where U_n is the identity matrix, and k^{-1}, k^*, $y = y^*$ are given by:

$$k^{-1} = \begin{bmatrix} \sqrt{Z_0} & 0 & 0 \\ 0 & \sqrt{Z_1} & 0 \\ 0 & 0 & \sqrt{Z_1} \end{bmatrix}$$

$$k^* = \begin{bmatrix} 1/\sqrt{Z_0} & 0 & 0 \\ 0 & 1/\sqrt{Z_1} & 0 \\ 0 & 0 & 1/\sqrt{Z_1} \end{bmatrix}$$

$$y^* = \begin{bmatrix} 1/Z_0 & 0 & 0 \\ 0 & 1/Z_1 & 0 \\ 0 & 0 & 1/Z_1 \end{bmatrix} \quad (4)$$

Now, the admittance matrix of the IC with input impedance Z_{IC} can be given as:

$$[Y]_{IC} = \begin{bmatrix} 0 & 0 & 0 \\ 0 & \frac{1}{Z_{IC}} & \frac{1}{Z_{IC}} \\ 0 & \frac{1}{Z_{IC}} & \frac{1}{Z_{IC}} \end{bmatrix} \quad (5)$$

Therefore, Y-matrix of the isolated balun can be calculated from equations (3) and (5) as:

$$[Y]_{\text{with IC}} = [Y]_{\text{without IC}} + [Y]_{IC} = \begin{bmatrix} 0 & \frac{-j}{\sqrt{2Z_0Z_1}} & \frac{j}{\sqrt{2Z_0Z_1}} \\ \frac{-j}{\sqrt{2Z_0Z_1}} & \frac{1}{Z_{IC}} & \frac{1}{Z_{IC}} \\ \frac{j}{\sqrt{2Z_0Z_1}} & \frac{1}{Z_{IC}} & \frac{1}{Z_{IC}} \end{bmatrix} \quad (6)$$

which in S-parameters reads as:

$$[S]_{\text{with IC}} = -k(Y+y)^{-1}(Y-y^*)k^{-1} = \begin{bmatrix} 0 & \frac{j}{\sqrt{2}} & \frac{-j}{\sqrt{2}} \\ \frac{j}{\sqrt{2}} & \frac{1}{2Z_1/Z_{IC}} - 1 & \frac{1}{2Z_1/Z_{IC}} - 1 \\ \frac{-j}{\sqrt{2}} & \frac{1}{2Z_1/Z_{IC}} - 1 & \frac{1}{2Z_1/Z_{IC}} - 1 \end{bmatrix} \quad (7)$$

Comparison of equations (2) and (5) shows that the IC does not, theoretically, have any effect on the balun insertion losses (S_{21}, S_{31}). Moreover, from equation (7) "perfect" output match and isolation can be achieved if $2Z_1 = Z_{IC}$ is satisfied.

Analysis of the wideband IC

Given the 180° phase difference between ports 2 and 3 in the balun, the IC can be realized by a $\lambda/2$ TL as depicted in Fig. 3(a). For this phase difference, a single $\lambda/2$ TL offers a limited bandwidth (see Fig. 3), and so we try here to provide analysis that results into a wideband IC. Figure 3 shows two different ICs; one with a TL of length $l_0 = \lambda_0/2$ (Fig. 3(a)), and the other with two TLs of lengths $l_1 = \lambda_1/2$, and $l_2 = \lambda_2/2$ (Fig. 3(b)).

In Fig. 3(a), input impedance Z_{in} of the IC's constituent TL with characteristic impedance Z_s can be calculated using equation (8):

$$Z_{in} = Z_s \frac{Z_1 + jZ_s\tan\frac{2\pi l_0}{\lambda}}{Z_s + jZ_1\tan\frac{2\pi l_0}{\lambda}} = Z_s \frac{Z_1 + jZ_s\tan\frac{\pi\lambda_0}{\lambda}}{Z_s + jZ_i\tan\frac{\pi\lambda_0}{\lambda}} = Z_s \frac{Z_1 + jZ_s\tan\frac{\pi\omega}{\omega_0}}{Z_s + jZ_1\tan\frac{\pi\omega}{\omega_0}} \quad (8)$$

where ω_0 is the center frequency, and ω is operating frequency.

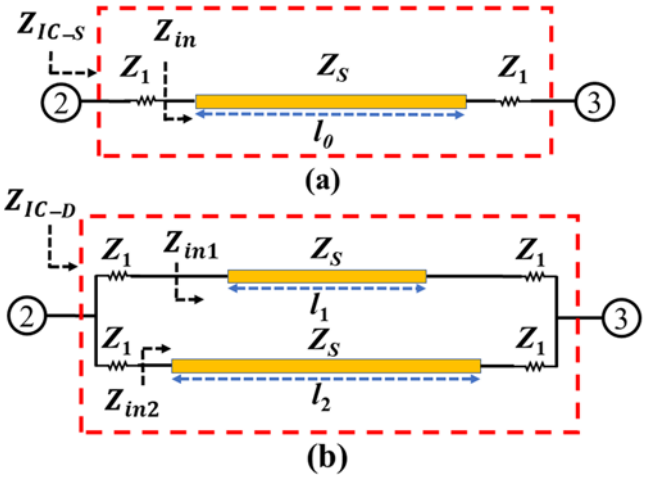

Figure 3. (a) Conventional IC and (b) the proposed IC.

The input impedance of the single-TL IC, $Z_{IC\text{-}S}$, can be given by:

$$Z_{IC\text{-}S} = Z_1 + Z_{in} \quad (9)$$

Now for very small bandwidth, $\Delta\omega_0$, around ω_0, let $\omega = \omega_0 + \Delta\omega_0$. Thus, bandwidth of the IC of Fig. 3(a) can be derived by calculating $Z_{IC\text{-}S}$:

$$Z_{IC\text{-}S} \cong \frac{Z_s^2 - Z_1^2 + Z_1Z_s}{Z_s} + j\left(\frac{Z_s^2 - Z_1^2}{Z_s}\right)\frac{\pi(\omega - \omega_0)}{\omega_0} \quad (10)$$

Fractional bandwidth (FBW) of IC in Fig. 3(a) can be obtained from equation (10) as:

$$\frac{2\Delta\omega_0}{\omega_0} = \frac{2}{\pi}\left(1 + \frac{Z_1Z_s}{Z_s^2 - Z_1^2}\right) \quad (11)$$

Therefore, to obtain maximum bandwidth in a single-TL IC, according to equation (11), one has to choose Z_S close to Z_1. For the case of a PA, where Z_1 (and in turn Z_S) is small, realizing correspondingly thick TL proves almost impractical.

Now, assuming $\omega = \omega_1 + \Delta\omega_1$ and $\omega = \omega_2 + \Delta\omega_2$, Z_{inm} (where $m = 1, 2$), Z_{inm} for the double-TL IC can be given by:

$$Z_{in_m} = Z_s \frac{Z_i + jZ_s\tan\frac{\pi\lambda_m}{\lambda}}{Z_s + jZ_i\tan\frac{\pi\lambda_m}{\lambda}} = Z_s \frac{Z_1 + jZ_s\tan\frac{\pi\omega}{\omega_m}}{Z_s + jZ_1\tan\frac{\pi\omega}{\omega_m}} \quad (12)$$

$$Z_{in_m} \cong \frac{Z_s^2 - Z_1^2 + Z_1Z_s}{Z_s} + j\left(\frac{Z_s^2 - Z_1^2}{Z_s}\right)\frac{\pi(\omega - \omega_m)}{\omega_m} \quad (13)$$

Therefore, $Z_{IC\text{-}D}$ for Fig. 3(b) can be calculated as:

$$Z_{IC\text{-}D} = ((Z_1 + Z_{in1})(Z_1 + Z_{in2}))/(2Z_1 + Z_{in1} + Z_{in2}) \quad (14)$$

Substituting equation (13) into (14) gives:

$$Z_{IC\text{-}D} \cong \frac{Z_0}{2}\left(1 + j\pi\left(\frac{(\omega - \omega_1)}{\omega_1} + \frac{(\omega - \omega_2)}{\omega_2}\right) \times \left(\frac{Z_s^2 - Z_1^2 - Z_1Z_s}{2(Z_s^2 - Z_1^2 + Z_1Z_s)}\right)\right) \quad (15)$$

https://doi.org/10.1017/S1759078724000709 Published online by Cambridge University Press

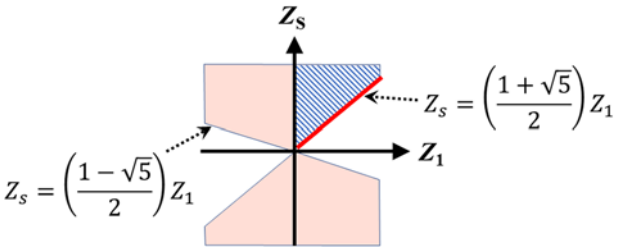

Figure 4. The hatched region indicates the permitted values of Z_S and Z_1 for the IC of Figure 3(b).

Assuming $\Delta\omega_1 \approx \Delta\omega_2$, the resonance frequency of the IC of Fig. 3(b) and its FBW can be determined as equation (16):

$$\frac{2\Delta\omega}{\omega_r} = \frac{4}{t\pi}\frac{Z_s^2 - Z_1^2 + Z_1Z_s}{Z_s^2 - Z_1^2 - Z_1Z_s} = \frac{4}{t\pi}\left(1 + \frac{Z_1Z_s}{Z_s^2 - Z_1^2 - Z_1Z_s}\right),$$
$$\omega_r = \frac{2\omega_1\omega_2}{\omega_1 + \omega_2} \tag{16}$$

Now, the bandwidth advantage of the proposed IC of Fig. 3(b) over IC of Fig. 3(a) becomes clear by dividing FBWs such that:

$$\frac{BW_{Double\text{-}TL}}{BW_{Single\text{-}TL}} = 2\left(1 + \frac{Z_1Z_s}{Z_s^2 - Z_1^2 - Z_1Z_s}\right) \tag{17}$$

Let $A = Z_s^2 - Z_1^2 - Z_1Z_s$; provided that $A > 0$, then, the FBW of double-TL IC of Fig. 3(b) will be at least twice that of the single-TL IC of Fig. 3(a). For $A > 0$ to be true, Z_S is derived in terms of Z_1 (see equation (18)) and plotted against it in Fig. 4. The hatched area shows the region that permits positive sign for A. That is, for the proposed double-TL IC and for a given Z_1, the corresponding Z_S can be obtained in this area, which guarantees at least doubled bandwidth compared to a single-TL IC. Note that the red line indicates the minimum values that Z_S can take for given Z_1 under this condition.

$$(Z_s - (\frac{1+\sqrt{5}}{2})Z_1)(Z_s - (\frac{1-\sqrt{5}}{2})Z_1)0 \tag{18}$$

Let's for a PA application, assume $Z_1 = 6\ \Omega$; then according to Fig. 4, $Z_s - (\frac{1+\sqrt{5}}{2})Z_1 0$ is forced (above the red line within the hatched area), which for the given Z_1 translates into $Z_S > 9.7\ \Omega$. This means that according to equation (17), in principle, for practical Z_S values (between 10 Ω and 100 Ω), a double-TL IC can offer a BW around 2.1–96.83 times the BW of the single-TL IC.

Here, a practical case of $Z_S = 25\ \Omega$ is selected for the sake of argument. Equation (17) ensures that the bandwidth of IC of Fig. 3(b) is approximately 2.7 times larger than that of the IC of Fig. 3(a). Now, we can verify this numerically. If we calculate $Z_{IC\text{-}S}$, and $Z_{IC\text{-}D}$ from equations (9) and (14) and substitute for isolation ($S_{32} = S_{23}$) in the matrix of equation (7), then we can plot isolation versus frequency for single-TL IC of Fig. 3(a) against double-TL IC of Fig. 3(b). As is evident in Fig. 5, the double-TL IC (red starred solid line) offers 3.2 times (with reference to −20 dB return loss (RL) level) larger bandwidth than single-TL IC (blue circled solid line). To further verify the results, both ICs of Fig. 3 are simulated in AWR Microwave Office software and isolation results are plotted in Fig. 5. Note that the results are in very good agreement. Furthermore, S_{23} of the classical BCD balun (i.e. without an IC) is also plotted in Fig. 5 against single-TL and double-TL cases, and as

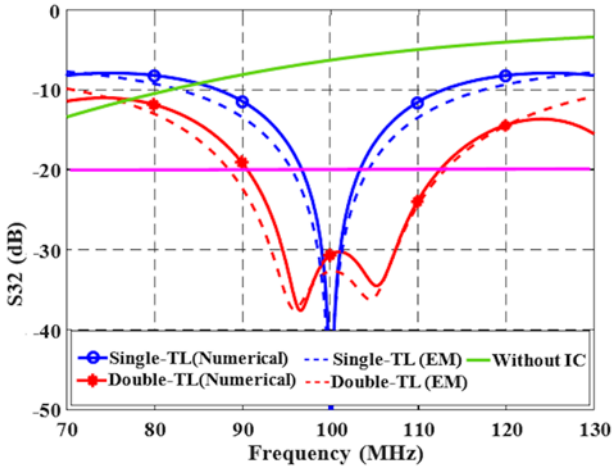

Figure 5. Isolation of single-TL IC against the proposed double-TL IC.

seen below, the S_{23} of balun without IC is very poor throughout the band, and in particular around the center frequency (and upward). Adding a single-TL IC improves this response and evidently, the double-TL IC improves the S_{23} significantly.

From a design perspective, the $\lambda/2$ length of the IC compared to the compact size of the balun itself, poses a size challenge, and so, it is essential to make the IC compact. This is done by using the equivalent T-network of the IC TLs loaded with shunt capacitors as shown in Fig. 6.

Design of the isolated BCB

Design procedure

Now that different blocks of the isolated BCB are analyzed, design of the proposed balun can be elaborated through a simple straightforward procedure, depicted in the flowchart of Fig. 7.

Note that the actual design involves much more details to be seen, and that since an all-ports-matched balun suitable for PA applications is intended, the procedure is presented by means of a balun that satisfies the PA requirements.

Case study: isolated balun design for PA applications

Design formulas and considerations for isolated BCB is illustrated through an example based on balun in Fig. 8.

For the BCB balun of Fig. 8(a) at f_c, the constitutive parameters of Fig. 2 are derived by:

$$f_c = \frac{1}{2\pi\sqrt{(C_m/2)(L_P + nL_m) - (1/4)(Z_1C_m)^2(1+n)}} \tag{19}$$

where $n = \sqrt{Z_0/2Z_1}$, and L_P and L_S in nH can be found from [22]:

$$L_{spiral} = L_P = L_S = \frac{1.27\mu_0N^2d_a}{2}\left(\ln\left(\frac{2.07}{\rho}\right) + 0.18\rho + 0.13\rho^2\right) \tag{20}$$

where $d_a = \frac{d_o+d_i}{2}$, $\rho = \frac{d_o-d_i}{d_o+d_i}$, N is the number of turns, and d_o, d_i are the outer and inner diameters of the coil, respectively (see Fig. 8(b)). In addition, for the stacked overlay spiral, C_m which is

https://doi.org/10.1017/S1759078724000709 Published online by Cambridge University Press

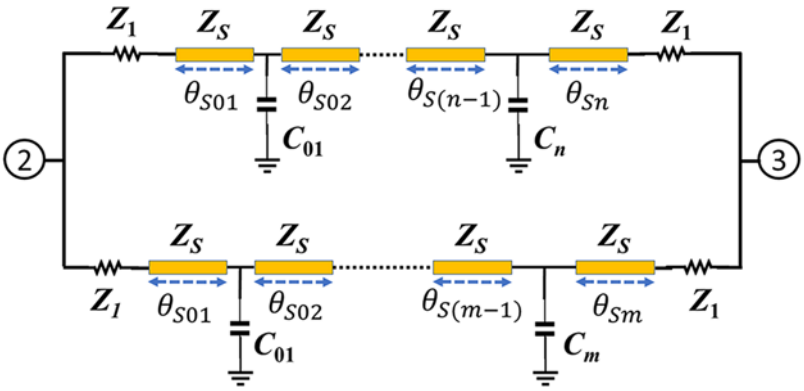

Figure 6. Equivalent circuit of double-TL ICs formed of shunt loaded capacitors.

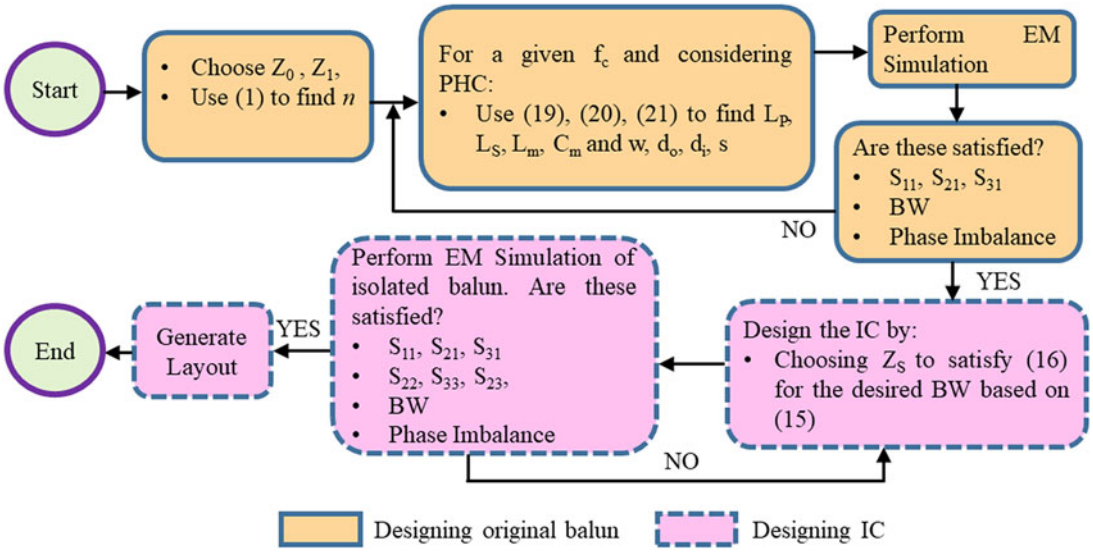

Figure 7. Design procedure for the proposed isolated broadside-coupled balun.

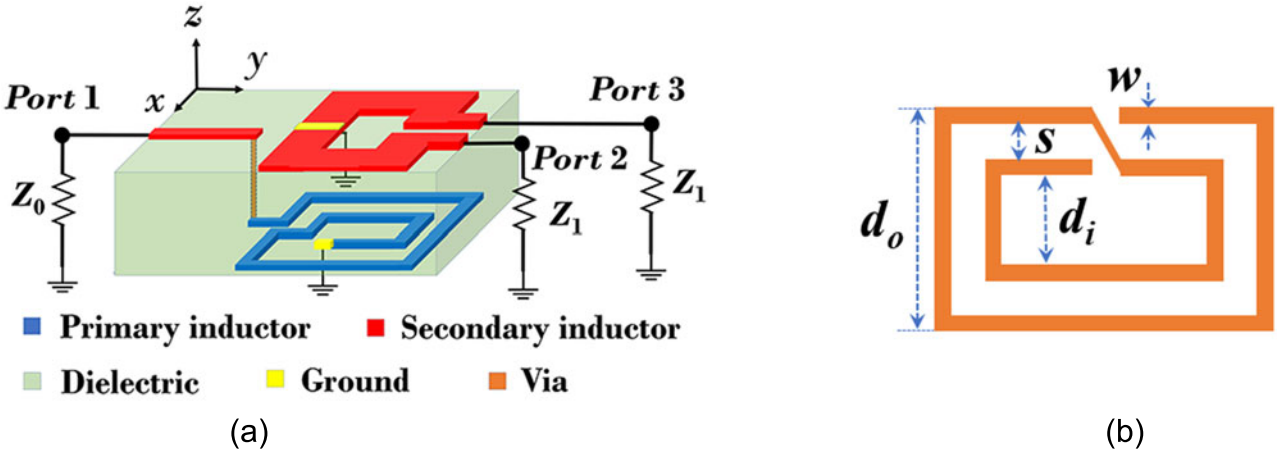

Figure 8. (a) 3D view of the BCB without isolation circuit: primary (blue), and secondary (red) windings sandwiching the substrate, and (b) associated geometrical parameters of spiral inductor.

https://doi.org/10.1017/S1759078724000709 Published online by Cambridge University Press

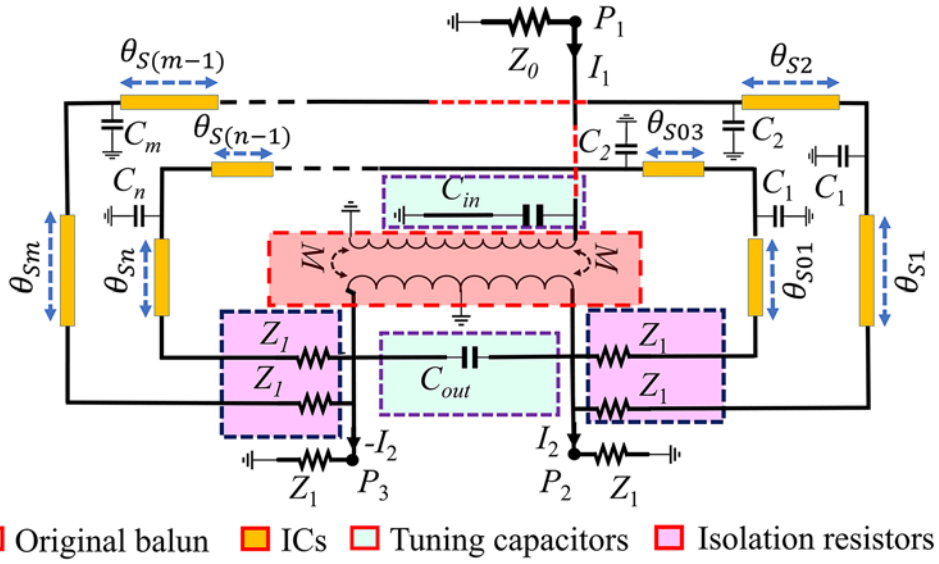

Figure 9. Schematic of the final isolated broadside-coupled balun.

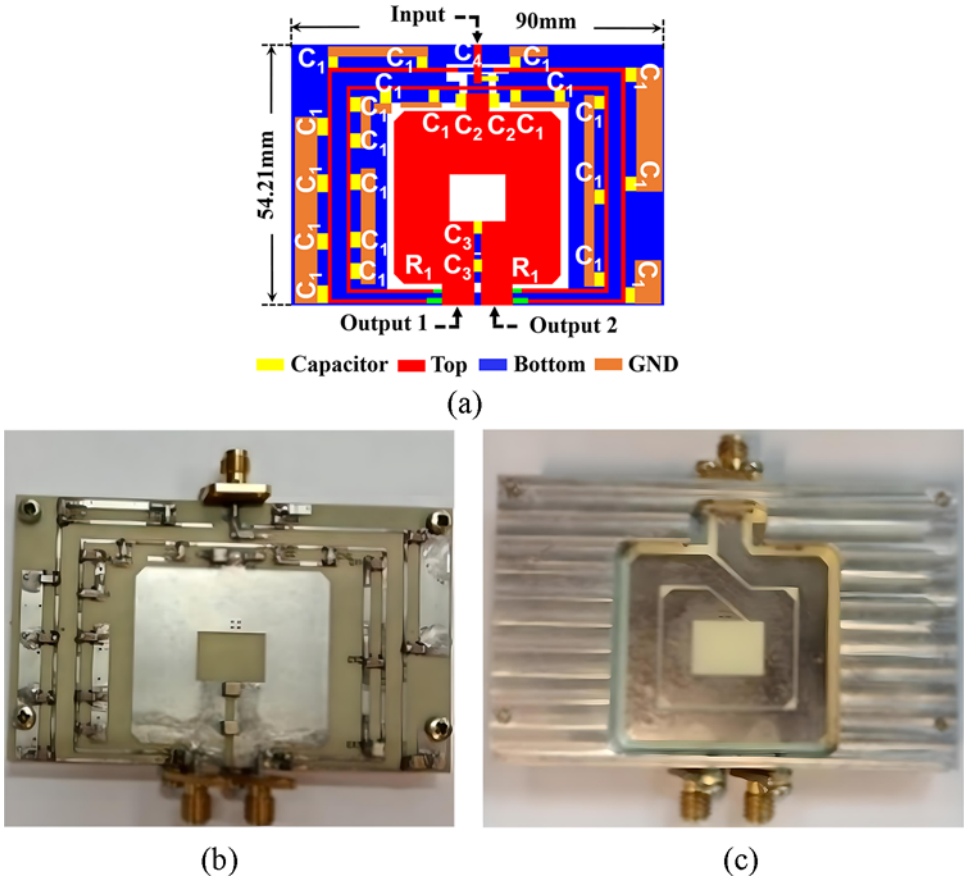

Figure 10. (a) Top view of the layout of balun, and photograph of (b) top and (c) bottom views of the fabricated balun.

proportional to the area occupied by the transformer can be found by [23]:

$$C_m = \frac{1}{2}\frac{\varepsilon_0 \varepsilon_r}{h}.\left(d_o{}^2 - d_i{}^2\right) \tag{21}$$

where h, and ε_r are the substrate thickness, and dielectric constant, respectively.

Also, according to equation (1), L_m can be determined in terms of K_m, L_S, and L_P as $L_m = K_m\sqrt{L_P L_S}$. The value of K_m mostly depends on the geometry of windings and h. While K_m for perfect coupling is unity, it is less than unity in practice. The value of K_m for broadside-coupled structures, which can be calculated from $K_m \approx 0.9 - h/AD$ for average diameter of AD, is

https://doi.org/10.1017/S1759078724000709 Published online by Cambridge University Press

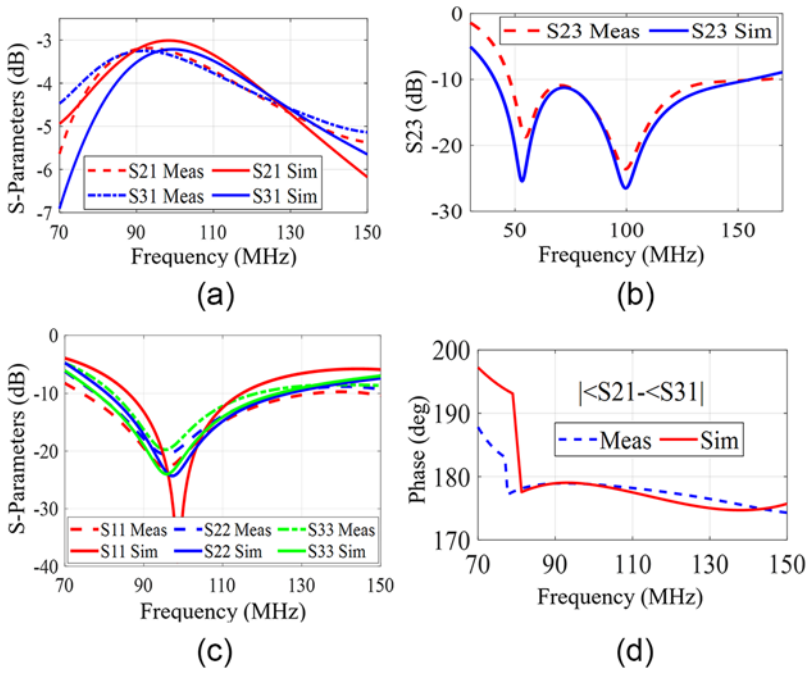

Figure 11. Comparison of full-wave simulation, and measurement results of balun in terms of (a) transmission, (b) isolation, (c) reflection, and (d) phase difference.

Table 1. Comparison with other similar published works

Reference	This work	[25]	[13]	[5]	[12]
f_0 (GHz)/FBW (%)	0.097/27	0.7/35	1.5/30	0.95/40	1.5/30
Insertion loss (dB)	3.8	3.32	NR	NR	3.5
Amplitude/phase imbalance (dB/°)	0.2/2	0.5/1.2	0.5/5	NR/NR	1/5
S_{23} (FBW at −10 dB)	118	40	NR	50	90
S_{11} (FBW at −10 dB)	50	40	30	60	45
S_{22} (FBW at −10 dB)	50	40	NR	50	45
S_{33} (FBW at −10 dB)	40	NR	NR	50	45
Dielectric constant	3.55	2.33	4.4	2.94	4.5
Relative size ($\lambda_g \times \lambda_g$)	0.03 × 0.06	0.12 × 0.03	0.11 × 0.11	0.63 × 0.47	NR
Input impedance (Ω)	50	NR	50	50	50
Output impedance (Ω)	6.25	NR	50	$16 + 0.6j$	40
Topology	BCB	MB	LDB	MLB	MB

Note: BCB = broadside-coupled balun; LDB = lumped-distributed balun; MB = Marchand balun; MLB = microstrip line balun, NR = not reported.

empirically reported to be mostly between 0.7 and 0.9 for strong coupling [24].

In PAs, large step-down impedance transformation ratio is desirable. For one thing, most PAs have low output resistance; in most cases, less than 10 Ω (depending on device voltage and power rating). Here, an isolated balun is designed to have 4:1 impedance transformation, i.e. $n = 2$. At $f_c = 97$ MHz and for $Z_0 = 50\ \Omega$ and $2Z_1 = 12.5\ \Omega$, number of turns for primary and secondary windings can be calculated from equation (1) as $N_P = 2, N_S = 1$. In other words, assuming perfect coupling, $K_m = 1$, based on equation (2), $L_P/L_S = 4$. Moreover, assuming $d_o = 38$ mm, $d_i = 10$ mm, geometrical and circuit model parameters are calculated using equations (19)–(21) to be $L_P = 108.4$ nH, $L_S = 27.11$ nH, $C_m = 26.4$ pF, $w_P = 12$ mm, $w_S = 5.5$ mm, $S = 0.7$ mm. At this stage, the IC is designed and added to the balun. The optimized IC parameters are obtained using Fig. 4 and equation (18) as $Z_S = 80\ \Omega$, $C_1 = 18$ pF, $C_2 = 1.3$ nF, $C_3 = 68$ pF, $C_4 = 1.2$ pF, $R_1 = 6.25\ \Omega$. The final schematic of the proposed isolated BCB is depicted in Fig. 9.

There are also some PHC constraints in choosing design parameters. More specifically, increasing substrate thickness, h, will improve PHC. Moreover, tracks should be wide enough to have suitable current-handling for the transistor. Maximum power rating of the isolation resistors (R_1–R_4) should be taken into account when determining the balun output power. For instance, here for a 100 W PA, each resistor should at least withstand 25 W for a robust design. Furthermore, tuning capacitors are used at input and output of the balun to improve phase and amplitude imbalance, insertion loss, and input return loss; though frequency shifting effect of such capacitors cannot be neglected.

https://doi.org/10.1017/S1759078724000709 Published online by Cambridge University Press

Simulation and measurement

To validate the proposed approach, the balun designed in the previous section is simulated in HFSS and fabricated on Rogers RO4003C substrate with $\varepsilon_r = 3.55$, $h = 0.8$ mm, and loss tangent Tan$D = 0.0027$. Figure 10(a) shows the top view of the balun layout, and Fig. 10(b) and (c) illustrate photographs of top and bottom sides of balun PCB. The very close agreement between calculated, simulation and measurement results demonstrate the validity of the proposed approach and accuracy of the computation and design.

Figure 11 shows the result of HFSS full-wave simulation against measurement, which covers the frequency range of the balun in 84–110 MHz, with input and output return losses of better than 11 dB, magnitude imbalance ($|S_{31}| - |S_{21}|$) of less than 0.2 dB, and phase imbalance better than 2°.

At this stage, it is essential to provide a comparative analysis of benefits and deficiencies of the proposed balun against other similar reported works. However, in this particular case, the variety in balun topologies for different applications and operating frequencies makes it quite challenging to do an analogous comparison. Therefore, performance of the balun presented here is compared to similar published works in Table 1.

As is evident, the proposed isolated balun outperforms other similar works in almost all design parameters. For instance, in terms of sizes versus bandwidths, the fabricated prototype can be claimed as the best and the smallest ever recorded using microstrip technology (even 50% smaller than [25]). Moreover, the 10 dB FBW of isolation, S_{23}, of 108%, and the amplitude imbalance, $|S_{21} - S_{31}|$, of 0.2 dB for the fabricated prototype are unbeatable in the literature. Furthermore, fabricated balun has the highest step-down impedance conversion desirable in PA applications compare to similar reported works. This is significant because the conversion rate greatly limits the bandwidth, while a reasonable bandwidth has been achieved with the proposed balun.

Conclusion

In this paper, an all-ports-matched multilayer BCB with arbitrary impedance transformation ratio was presented. Analysis of the isolated BCB and that of its constituent wideband IC was demonstrated. Frequency response of the proposed IC is evaluated analytically and verified numerically, confirming its wide FBW. In addition, a simple straightforward procedure for design of the isolated multilayer balun was presented that offers a guaranteed optimum design through clear steps. The proposed low-profile balun is fabricated and measured using E5071C VNA. The performance of the balun, and particularly the isolation between output ports (S_{23}) at FBW = 118%, not only confirms the validity of the proposed approach, but also makes the balun a competent alternative to the existing ones, particularly for PA applications.

Competing interests. The authors report no conflict of interest.

References

1. **Chen H-S, Wu C-H, Lin Y-C and Liu JY-C** (2017) A K-band area-saving Marchand balun integrated with low-noise amplifier in 0.18-μm CMOS. In *2017 IEEE Asia Pacific Microwave Conference (APMC)*, IEEE, 1196–1199.
2. **Mannem NS, Huang T-Y and Wang H** (2021) Broadband active load-modulation power amplification using coupled-line baluns: A multi-frequency role-exchange coupler Doherty amplifier architecture. *IEEE Journal of Solid-State Circuits* **56**(10), 3109–3122.
3. **Smith R and Cripps SC** (2016) Broadband push-pull power amplifier design at microwave frequencies. In *2016 46th European Microwave Conference (EuMC)*, IEEE, 1353–1356.
4. **Chongcheawchamnan M, Ang K, Wong J and Robertson I** (2000) A push-pull power amplifier using novel impedance-transforming baluns. In *2000 30th European Microwave Conference*, IEEE, 1–4.
5. **Maktoomi MH, Ren H, Marbell MN, Klein V, Wilson R and Arigong B** (2020) A wideband isolated real-to-complex impedance transforming uniplanar microstrip line balun for push–pull power amplifier. *IEEE Transactions on Microwave Theory & Techniques* **68**(11), 4560–4569.
6. **Zhang W, Wu Y, Yu C and Chen W** (2015) Compact coupled-line balun with complex impedances transformation and high isolation. *IET Microwaves, Antennas & Propagation* **9**(14), 1587–1594.
7. **Moghaddam ES and Ahmadi A** (2020) 180° hybrid using a novel planar balun on suspended substrate for beam forming network applications. *International Journal of RF and Microwave Computer-Aided Engineering* **30**(9), e22280.
8. **Sardin D and Popović Z** (2013) Decade bandwidth high-efficiency GaN VHF/UHF power amplifier. In *2013 IEEE MTT-S International Microwave Symposium Digest (MTT)*, IEEE, 1–3.
9. **Hsu H-M, Lai S-H and Hsu C-J** (2010) Compact layout of on-chip transformer. *IEEE Transactions on Electron Devices* **57**(5), 1076–1083.
10. **Yoon YJ, Lu Y, Frye RC, Lau MY, Smith PR, Ahlquist L and Kossives DP** (1999) Design and characterization of multilayer spiral transmission-line baluns. *IEEE Transactions on Microwave Theory & Techniques* **47**(9), 1841–1847.
11. **Ahn H-R and Nam S** (2011) New design formulas for impedance-transforming 3-dB Marchand baluns. *IEEE Transactions on Microwave Theory & Techniques* **59**(11), 2816–2823.
12. **Ang KS and Robertson ID** (2001) Analysis and design of impedance-transforming planar Marchand baluns. *IEEE Transactions on Microwave Theory & Techniques* **49**(2), 402–406.
13. **Ang KS, Leong YC and Lee CH** (2003) Analysis and design of miniaturized lumped-distributed impedance-transforming baluns. *IEEE Transactions on Microwave Theory & Techniques* **51**(3), 1009–1017.
14. **Xu J-X, Zhang XY and Zhao X-L** (2016) Compact LTCC balun with bandpass response based on Marchand balun. *IEEE Microwave and Wireless Components Letters* **26**(7), 493–495.
15. **Zhou T, Yang G-L, Chen R, Zhang H and Wang K** (2021) Design of a wideband CMOS balun and its application in a wideband RF front-end. *IEEE Access* **9**, 94416–94425.
16. **Chiou H-K and Liao H-Y** (2010) Broadband and low-loss 1:9 transmission-line transformer in 0.18-μm CMOS process. *IEEE Electron Device Letters* **31**(9), 921–923.
17. **Ahn H-R and Itoh T** (2010) New isolation circuits of compact impedance-transforming 3-dB baluns for theoretically perfect isolation and matching. *IEEE Transactions on Microwave Theory & Techniques* **58**(12), 3892–3902.
18. **Long JR** (2000) Monolithic transformers for silicon RF IC design. *IEEE Journal of Solid-State Circuits* **35**(9), 1368–1382.
19. **Ma K, Yan N, Yeo KS and Lim WM** (2014) Miniaturized 40–60 GHz on-chip balun with capacitive loading compensation. *IEEE Electron Device Letters* **35**(4), 434–436.
20. **Jaisson D** (1999) Planar impedance transformer. *IEEE Transactions on Microwave Theory and Techniques* **47**(5), 592–595.
21. **Abrie PL** (1999) *Design of RF and Microwave Amplifiers and Oscillators*. Boston, MA: Artech House.
22. **Mohan SS, Del Mar Hershenson M, Boyd SP and Lee TH** (1999) Simple accurate expressions for planar spiral inductances. *IEEE Journal of Solid-state Circuits* **34**(10), 1419–1424.
23. **Yue CP and Wong SS** (2000) Physical modeling of spiral inductors on silicon. *IEEE Transactions on Electron Devices* **47**(3), 560–568.
24. **Mohan SS, Yue CP, Del Mar Hershenson M, Wong SS and Lee TH** (1998) Modeling and characterization of on-chip transformers. In *International Electron Devices Meeting 1998*. Technical Digest (Cat. No. 98CH36217), IEEE, 531–534.
25. **Ahn H-R and Tentzeris MM** (2019) A novel compact isolation circuit suitable for ultracompact and wideband Marchand baluns. *IEEE Transactions on Circuits and Systems II: Express Briefs* **67**(10), 2299–2303.

https://doi.org/10.1017/S1759078724000709 Published online by Cambridge University Press

Masoud Farhadinia received the M.Sc. degree in telecommunication engineering from Shahid Beheshti University, Tehran, Iran, in 2017. He is currently working as an RF HW developer and researcher with NAK Telecom Company, Tehran, Iran. His current research interests include wireless communications, linear and high efficiency power amplifier, and RF energy harvesting.

Dr. Esfandiar Mehrshahi was born in Tehran, Iran 1964. He received his B.Sc. from Iran University of Science and Technology, Tehran, Iran, in 1987, and the M.Sc. and Ph.D. degrees from Sharif University of Technology, Tehran, Iran, in 1991 and 1998, respectively. Since 1990 he has been involved in several research and engineering projects at the Iran Telecommunications Research Centre (ITRC). He is currently an Associate Professor at Shahid Beheshti University, Tehran, Iran. His main areas of interest are nonlinear simulation of microwave circuits and microwave oscillator's spectrum.

Dr. Shokrollah Karimian is an Assistant Professor in School of Electrical Engineering at Shahid Beheshti University. As a member of IEEE, with over 70 publications, he has made a valuable contribution to the RF and microwave/mm-wave community.

https://doi.org/10.1017/S1759078724000709 Published online by Cambridge University Press